Mass-resolved VUV laser spectroscopy of XeAr: Two competing predissociation pathways in the *C*1 state

Shilin Liu, Akiyoshi Hishikawa, and Kaoru Yamanouchi[a)]
Department of Chemistry, School of Science, The University of Tokyo, 7-3-1 Hongo, Bunkyo-ku, Tokyo 113-0033, Japan

(Received 3 December 1997; accepted 24 December 1997)

Mass-resolved excitation spectra of the $C1-X0^+$ band of XeAr were measured under jet-cooled conditions using a tunable coherent vacuum ultraviolet (VUV) light ($\lambda \sim 130$ nm) as an excitation light source and a high-resolution ($m/\Delta m \sim 1100$) reflectron time-of-flight mass spectrometer. The rotational structure of the $C1-X0^+$ $(v',0)$ $(v'=2-6)$ vibronic bands were recorded by monitoring the parent $^{132}Xe^{40}Ar^+$ ions and the fragment $^{132}Xe^+$ ions. From the analysis of the rotational structures, the existence of the two dissociation pathways from the $C1$ state was identified for the first time; i.e., (i) the rotationally dependent predissociation caused by an electron-rotation interaction (**L**- and/or **S**-uncoupling) with the dissociative state with 0^- symmetry correlating with the Xe $6s'(1/2)_0$ level, and (ii) the rotationally independent predissociation caused by the electrostatic interaction with a repulsive state with $\Omega=1$ symmetry correlated either with the Xe $6s(3/2)_1$ level or the Xe $6s(3/2)_2$ level. From the least-squares fit to the partially resolved rotational structures, the dissociation rates for these two pathways as well as the band origins and the rotational constants, were derived for the $v'=2-6$ levels in the $C1$ state. © *1998 American Institute of Physics.* [S0021-9606(98)01513-X]

I. INTRODUCTION

Recent developments in a frequency up-conversion technique in laser spectroscopy have enabled us to investigate interatomic potentials of homonuclear[1–4] and heteronuclear[5–12] rare gas dimers in the electronically excited states, which are located in the VUV wavelength region. Among the heteronuclear rare gas dimers, XeRg (Rg =Ne, Ar, and Kr) dimers have been studied most intensively. So far, their interatomic potentials correlated with the $6s(3/2)_1$,[5,6,9,12] $6s'(1/2)_1$,[5,6,8] $6p(5/2)_2$,[10,11] $6p(5/2)_3$,[7,10,11] $6p(3/2)_1$,[7,10,11] $6p(3/2)_2$,[5,7,10,11] and $6p(1/2)_0$[5,7,11] levels of Xe were investigated.

The first detailed spectroscopic analyses of the XeRg dimers were reported by Tsuchizawa, Yamanouchi, and Tsuchiya[8] with a tunable VUV laser generated by four-wave difference-frequency mixing in a nonlinear gaseous medium. They measured the VUV laser-induced fluorescence (LIF) excitation and the two-color resonantly enhanced two-photon ionization (RE2PI) spectra of XeNe, XeAr, and XeKr in a supersonic free jet in the wavelength region near the atomic transition of Xe$[6s'(1/2)_1 \leftarrow {}^1S_0]$ and found the two vibronic band systems. These two bands were assigned as the $C1-X0^+$ and the $D0^+-X0^+$ electronic transitions, and the interatomic potentials of the $C1$ state and the $D0^+$ state of XeAr and XeKr were determined. The electronic assignments of $\Omega=1$ to the C state and $\Omega=0^+$ to the D state were performed for XeAr by the simulation of the rotational contour of the vibronic transitions. These assignments were recently confirmed by Mao *et al.*[13] by measuring the one-color $(2+1)$ resonantly enhanced multiphoton ionization spectra using linearly and circularly polarized laser light.

Although the static properties of the electronically excited XeRg dimers, such as the transition energies and the interatomic potentials, have been reported precisely, no information has been known so far regarding their dynamical properties, i.e., dissociation processes in these excited states. In general, high-resolution measurements of the rotational structures of vibronic transitions often provide us with invaluable information concerning dissociation rates and an interaction with a nearby electronic state, which causes the dissociation. For XeRg, a detailed study of the rotational structure to extract the dissociation dynamics has been hindered by the two factors which made the rotational structure congested, i.e., (i) the heavy reduced mass and the long-bond length resulting in small rotational constants, and (ii) the overlapping rotational bands of a number of isotopic species with small isotope shifts.

In the present study, the predissociation dynamics in the $C1$ state of XeAr dimers is studied by measuring the partially resolved rotational structures of the $C1-X0^+$ vibronic transitions using a tunable coherent VUV light source with a frequency resolution of (~ 0.09 cm^{-1}) and a reflectron time-of-flight (TOF) mass spectrometer with a mass resolution of $m/\Delta m \sim 1100$. The mass-selected parent ^{132}XeAr* molecules as well as the fragment ^{132}Xe* atoms are monitored through the ionization process induced by a probe laser, which eliminates the isotopic spectral congestion. From the analysis of rotational structures of the mass-selected $C1-X0^+$ transition, two different predissociation pathways, i.e., homogeneous and heterogeneous pathways, have been identified for the first time, and their dissociation mechanisms are discussed.

[a)]Author to whom correspondence should be addressed.

II. EXPERIMENT

The present experimental setup consists of (i) a pulsed molecular beam source to generate the jet-cooled XeAr dimers, (ii) a narrow bandwidth ($\sim 0.09\ \mathrm{cm}^{-1}$) tunable coherent VUV laser light source in the wavelength region near the Xe[$6s'(1/2)_1 \leftarrow {}^1S_0$] transition ($\sim 130$ nm), and (iii) a high-resolution ($m/\Delta m \sim 1100$) reflectron TOF mass spectrometer.

The XeAr dimers were produced by the supersonic expansion of Xe/Ar/He rare gas mixture (Xe:Ar:He $\sim$0.1:10:90) through a pulsed nozzle (General Valve 9-279-900) with a nozzle orifice diameter of 0.2 mm into a main chamber. The main chamber was pumped by a 6″ oil diffusion pump (Edwards Diffstak MK-2, 63/700 M; 700 l/s) which is backed up by a rotary pump (ULVAC D-950, 950 l/min). The supersonic jet was collimated by a skimmer (3 mm ϕ) located 40 mm downstream from the nozzle orifice, and introduced into the laser–molecule interaction region, which was differentially pumped by a turbo molecular pump (Balzers/Pfeiffer Vacuum, TMU-1000; 920 l/s) with a rotary pump (950 l/min). The stagnation pressure was kept in a range of $3\sim5$ atm and the operating pressure in the main chamber was $\sim 10^{-5}$ Torr.

The tunable, coherent VUV light was generated by two-photon resonance four-wave difference frequency mixing of two dye laser lights in Kr.[14] Hereafter, we refer to this coherent VUV light source as a VUV laser. The frequency doubled output (ω_1) of the first dye laser was tuned to the two-photon resonant level of Kr $5p(1/2)_0$ at 940 93.662 cm^{-1},[15] while the wave number of the second dye laser output (ω_2) was continuously scanned in the wavelength region of 587–594 nm to generate the VUV laser output having the $2\omega_1-\omega_2$ wave number. These two dye lasers (Lambda Physik FL3002E) were simultaneously pumped by an excimer laser (Lambda Physik LPX205i). The two laser beams were merged coaxially by a dichroic mirror, and were focused by an achromatic lens with $f=300$ mm into a cell containing the Kr gas. The generated VUV laser beam in the 129.4–129.8 nm range was refocused by a MgF_2 lens ($f=180$ mm), and introduced into the main vacuum chamber after separated from the two laser beams with ω_1 and ω_2 wave numbers by a LiF prism.

After exciting XeAr to the $C1$ state by the VUV laser, the parent XeAr molecules in the $C1$ state and the Xe fragment atoms produced from the $C1$ state were ionized by an ionization laser with the wave number of $\omega_1/2$, which was separated from ω_1 laser light after the frequency doubling crystal (BBO) and was coaxially counterpropagated with the VUV laser beam. The optical delay of the ionization laser relative to the VUV laser was estimated to be around 3 ns by measuring the difference of the optical lengths from the position of the BBO crystal to the laser–molecule interaction point. Considering that the pulse width of the pumping excimer laser is about 28 ns, a secure temporal overlap between the VUV light and the probe laser was achieved at the laser–molecule interaction point.

After the dissociation of XeAr in the $C1$ state, the Xe fragment atoms could be produced energetically in four electronic states, i.e., three excited state, $6s'(1/2)_0$, $6s(3/2)_1$, and $6s(3/2)_2$, and the ground 5^1S_0 state, as shown in Fig. 1. In the present experiment, the produced Xe atom was probed by the ionization laser with the wave number of $\omega_1/2$. Therefore, Xe atoms in the electronic states with energies above I.P.(Xe)$-\omega_1/2$ can be ionized by the ionization laser, where I.P.(Xe) denotes the ionization potential of Xe. Among the four electronic states of Xe, only the $6s'(1/2)_0$ state is probed by the ionization laser, as illustrated in Fig. 1. The produced ions were extracted and accelerated into a time-of-flight (TOF) mass spectrometer (Comstock RTOF201) and drifted along a 1.5 m long TOF tube toward the reflectron, and after the reflection, the ions were detected by a microchannel plate (MCP) detector located 1 m downward from the reflectron. The signals from the MCP output were amplified with a preamplifier (PAR 115), and the mass-resolved data were collected by averaging the preamplified signals for selected mass species by boxcar averagers (Stanford SR250). Both the intensities of the VUV laser and the ionization laser were monitored during the experiment, and were averaged with boxcar averagers.

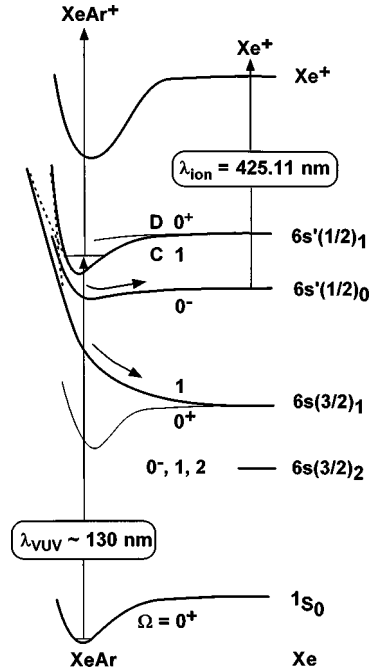

FIG. 1. A schematic energy diagram of XeAr. The dissociation pathways to form the four electronic states of Xe, i.e., $6s'(1/2)_0$, $6s(3/2)_1$, $6s(3/2)_2$, and ${}^1S_0$, are energetically open from the $C1$ state. In the present study, the fragment Xe atoms populated in the $6s'(1/2)_0$ state were selectively ionized by the ionization laser ($\lambda=425.11$ nm).

In order to estimate the resolution [fullwidth at half maximum (FWHM)] of the VUV laser light, the LIF excitation spectrum of the $A-X(9,0)$ ($\nu_0=768\,42.162\ \mathrm{cm}^{-1}$) band of CO[16] was recorded by the $1+1$ RE2PI scheme where the ω_1 laser is used as the ionization laser. From the measurements of the well-resolved single rotational linewidths, the VUV laser resolution was estimated to be $0.30\ \mathrm{cm}^{-1}$ when both of the two dye lasers were operated in the grating-tuned mode, and $0.09\ \mathrm{cm}^{-1}$ with an intracavity etalon inserted for the ω_2 laser. The wave number of the ω_2 laser was calibrated by the LIF excitation spectrum of I_2,[17] which was measured

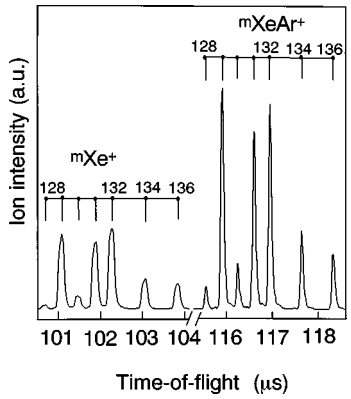

FIG. 2. The TOF mass spectrum averaged over 500 laser shots recorded by exciting the rotational band-head of the $C-X$ (4,0) transition at $\lambda_{\mathrm{VUV}}=129.6$ nm. The mass resolution was estimated to be $m/\Delta m=1100$ from the XeAr^+ spectra. The mass peaks for the Xe^+ ions exhibit broader peak widths due to the large released kinetic energy imposed on the Xe^+ ions after the dissociation.

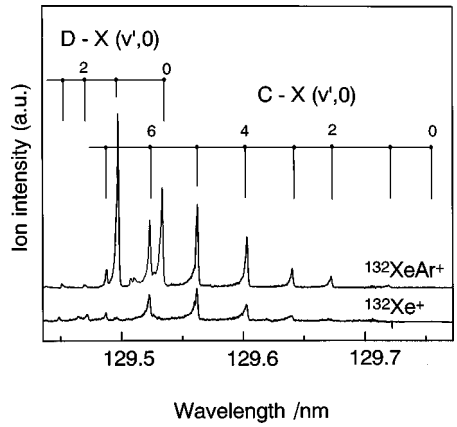

FIG. 3. The two excitation spectra obtained simultaneously by monitoring the $^{132}\mathrm{Xe}^{40}\mathrm{Ar}^+$ (upper trace) and $^{132}\mathrm{Xe}^+$ (lower trace) ions. The $C1-X0^+$ and $D0^+-X0^+$ bands are observed in the $^{132}\mathrm{Xe}^{40}\mathrm{Ar}^+$ spectrum,while only the $C1-X0^+$ band is visible in the $^{132}\mathrm{Xe}^+$ spectrum, indicating that Xe $6s'(1/2)_0$ is produced only from the $C1$ state in the observed energy range.

simultaneously throughout the experiment. It should be remarked that the two-photon transition wave number $2\omega_1$, which maximizes the output power of the VUV laser, differs slightly from the atomic level energy due to the phase matching in Kr. Therefore, the wave number of the generated VUV laser was calibrated with respect to the CO $A-X$ transition. The two-photon resonance energy $2\omega_1$ was determined from the wave number of the $Q(1)$ line (768 36.252 cm^{-1}) of the CO $A-X$ (9,0) band, and the wave number of the ω_2 laser was calibrated by the LIF spectra of I_2. The determined $2\omega_1$ was slightly smaller by 0.524 cm^{-1} than the energy difference between Kr $5p(1/2)_0$ and the ground state $^1S_0$. Thus, the excitation VUV wave number was calibrated according to the formula $\omega_{\mathrm{VUV}}=2\omega_1-\omega_2$ on the basis of the determined $2\omega_1$ value.

III. RESULTS AND DISCUSSION

A. Overall spectral features

Figure 2 shows the TOF mass spectrum obtained by fixing the wavelength of the VUV laser at $\lambda=129.6$ nm in the band-head region of the $C1-X0^+$ (4,0) band of XeAr. It is clearly seen in the mass spectrum that both the parent XeAr^+ ions and the Xe^+ fragment ions were produced at this VUV wavelength. The Xe^+ ions could originate either from (i) the dissociation in the intermediate $C1$ state of XeAr or (ii) the dissociation of the XeAr^+ ions produced after absorbing the $\omega_1/2$ laser light. In order to clarify the origin of the Xe^+ ions, the output of another excimer laser-pumped dye-laser system was used as the ionization laser ($\omega\sim\omega_1/2$) to vary the delay between the VUV laser and the ionization laser. When the ionization laser was delayed by more than 5 ns with respect to the VUV laser at the laser–molecule interaction point, only the Xe^+ fragments were observed. This observation excludes the latter possibility ''(ii)'' and indicates the presence of a photodissociation process in the XeAr $C1$ state to form Xe atoms in the $6s'(1/2)_0$ state.

In the mass spectrum, the seven abundant isotopic species of both the parent $^m\mathrm{Xe}^{40}\mathrm{Ar}^+$ and the fragment $^m\mathrm{Xe}^+$ ions ($m=128,129,130,131,132,134,136$) were completely separated from each other, and the mass resolution was estimated to be $m/\Delta m\sim1100$ from the ^{m}XeAr mass spectrum. The high mass-resolving power in our experiment enabled us to detect the mass-selected parent and fragment ions without isotopic congestion. It can be seen in Fig. 2 that the ^{m}Xe peaks were broader than the ^{m}XeAr peaks. From the rotational band origin, 771 59.67 cm^{-1},[8] of the $C-X$ (4,0) band and the dissociation energy of the electronic ground state of XeAr, 118.5 cm^{-1},[12] the released kinetic energy of the Xe $6s'(1/2)_0$ channel is calculated to be 844 cm^{-1}. The broader peaks in the Xe^+ mass spectrum may reflect the translational energy distribution of the atomic fragments formed after the dissociation process.

The upper trace of Fig. 3 shows the excitation spectrum obtained by monitoring the most abundant $^{132}\mathrm{Xe}^{40}\mathrm{Ar}^+$ parent ions (26.79%) in the wavelength region between 129.4 and 129.8 nm, where two band systems assigned as $C1-X0^+$ and $D0^+-X0^+$ transitions were observed. The observed spectral structures were in good agreement with those reported by Tsuchizawa *et al.*,[8] so that their vibrational assignments were adopted for these two band systems. On the other hand, in the spectrum obtained by monitoring the $^{132}\mathrm{Xe}^+$ fragment ions shown in the lower trace of Fig. 3, only the $C1-X0^+$ transitions were clearly identified, indicating that the Xe $6s'(1/2)_0$ fragments were dominantly produced from the $C1$ state of XeAr. At the wave number positions of the $D0^+-X0^+$ (2,0) and (3,0) transitions, two very weak peaks were also observed in this $^{132}\mathrm{Xe}^+$ spectrum. Since it has been known that the $D1u-X0_g^+$ (0,0) and (1,0) transitions of Xe_2 overlap, respectively, with those of the $D0^+-X0^+$ (2,0) and (3,0) transitions of XeAr,[18] these two weak peaks in the $^{132}\mathrm{Xe}^+$ spectrum were assigned to the $D-X$ (0,0) and (1,0) transitions of the Xe_2 dimers, which produce the Xe atoms in the $6s'(1/2)_0$ state.

B. Rotational structures and dissociation mechanism of the *C*1 state

In order to clarify the dissociation pathways and mechanisms in the $C1$ state, the rotational structures of the

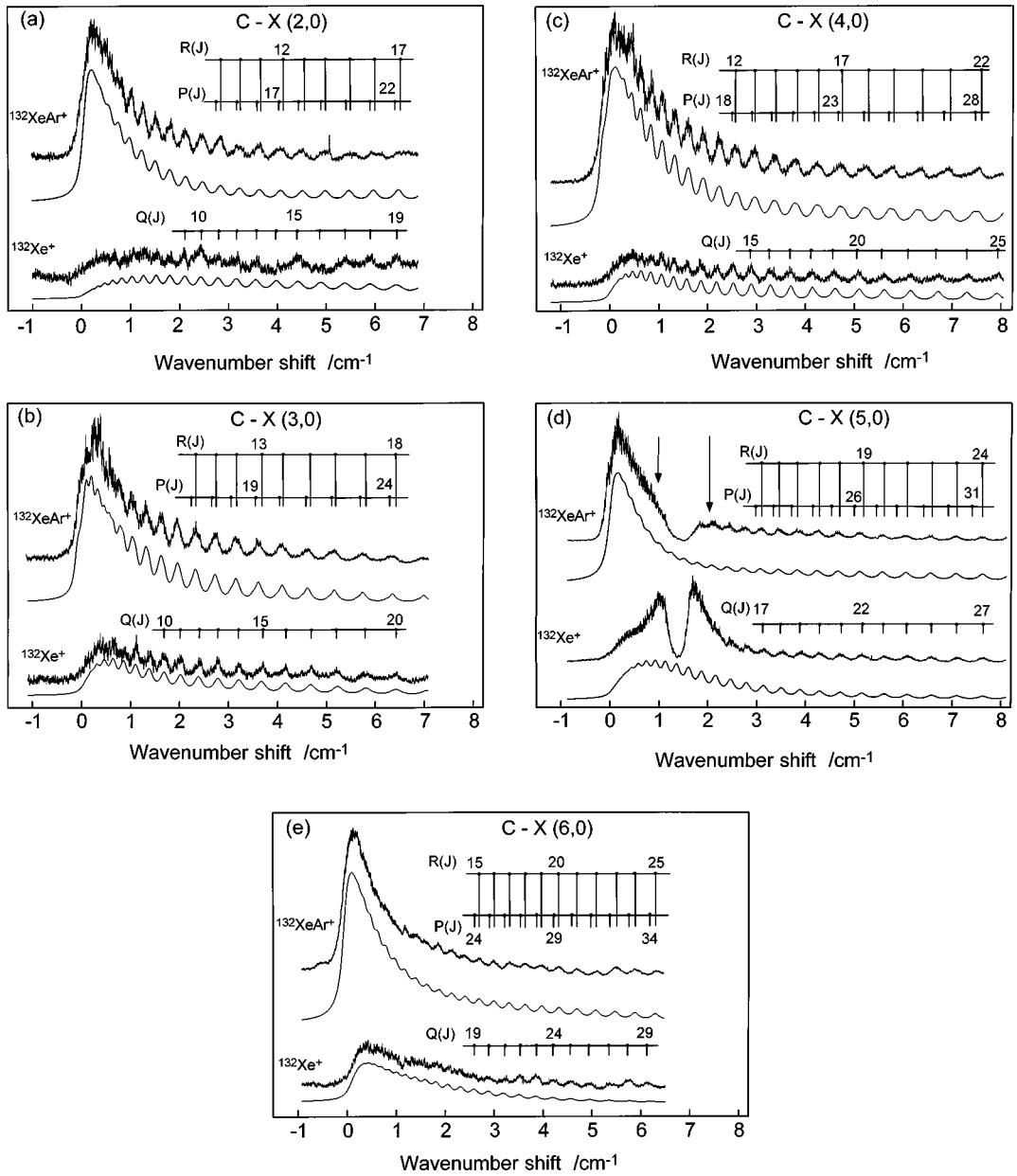

FIG. 4. The rotational structures of the $(v',0)$ $(v'=2-6)$ vibronic bands of the $C1-X0^+$ band observed by monitoring $^{132}Xe^{40}Ar^+$ (upper trace) and $^{132}Xe^+$ (lower trace); (a) $v'=2$, (b) $v'=3$, (c) $v'=4$, (d) $v'=5$, (e) $v'=6$. The simulated spectra obtained by the least-squares fit to the observed rotational structures are also shown in comparison with the experimental results. Due to the self-absorption effect at the strong atomic resonant transition $[6s'(1/2)_1 \leftarrow {}^1S_0]$ of the background Xe atoms, the spectral fit of the $C-X(5,0)$ band was performed only for the $^{132}Xe^{40}Ar^+$ spectrum by using the spectrum outside the energy region between the two arrows.

$(v',0)(v'=2-6)$ vibrational bands of the $C1-X0^+$ transition were measured with high-resolution ($\Delta\nu \sim 0.09\ \mathrm{cm}^{-1}$) by monitoring both the $^{132}Xe^{40}Ar^+$ and $^{132}Xe^+$ ions simultaneously. The observed rotational structures are shown in Figs. 4(a)–4(e), where the upper trace in each figure was obtained by monitoring the parent $^{132}Xe^{40}Ar^+$ ions and the lower trace by monitoring the fragment $^{132}Xe^+$ ions.

In the previous study,[8] the electronically excited C state of XeAr was classified as the $\Omega=1$ state using the Hund's case (c) coupling scheme on the basis of the existence of the P, Q, and R branches identified in the $C-X$ vibronic transitions, where Ω represents the projection of the total angular momentum onto the internuclear axis. Therefore each of the rotational levels in the $C1$ state consists of e- and f-parity components. The selection rules for the electronic dipole transition are given as: $e \leftrightarrow e$ and $f \leftrightarrow f$ for the P- and R-branch transitions, and $e \leftrightarrow f$ for the Q-branch transitions.[19] Since all the rotational levels in the electronic ground state 0^+ have e-parity, P- and R-branch transitions terminate at the rotational e-parity sublevels of the $C1$ state, while the Q-branch transitions terminate at the rotational f-parity sublevels.

By examining the rotational structures in Figs. 4(a)–4(e), it was found commonly in these spectra that the rotational peak positions of the spectra obtained by monitoring $^{132}Xe^+$ ions shifted by small amounts from those obtained by monitoring $^{132}Xe^{40}Ar^+$ ions. The spectral shift is most clearly identified in the (6,0) band of the $C1-X0^+$ transition

in Fig. 4(e). An analysis of the rotational structure of Fig. 4(e) showed that the spectrum obtained by monitoring the $^{132}Xe^+$ ion consists only of Q-branch transitions from the ground $\Omega=0^+$ state of XeAr. This evidence indicates that the ^{132}Xe fragments in the $6s'(1/2)_0$ level monitored in the present study are produced only from the f-parity rotational sublevels in the $C1$ state.

On the basis of the selection rules for perturbation,[19] $e\leftrightarrow e$ and $f\leftrightarrow f$, the dissociative electronic state which couples with the $C1$ state of XeAr should have the f-parity rotational levels, indicating that the perturbating electronic state possesses the $\Omega=0^-$ electronic symmetry. As shown schematically in Fig. 1, in the energy range investigated in the present study, there exists only one $\Omega=0^-$ electronic state which can interact with the $C1$ state. The fact that this $\Omega=0^-$ state is correlated with Xe $6s'(1/2)_0$,[20] which was ionized and detected in the present study, supports the proposed dissociation pathway from the $C1$ state.

Further confirmation of this dissociation pathway from the $C1$ state can be obtained from the linewidth of the Q-branch rotational transitions. If the $\Omega=0^-$ state is assumed to be the perturber, the nonzero off-diagonal matrix elements of the rotational Hamiltonian exist between these two electronic states due to the **L**- and/or **S**-uncoupling terms. In such a case, the dissociation rate, which is proportional to the square-modulus of the matrix elements for the coupling terms, becomes proportional to $J'(J'+1)$. It can be seen in the $^{132}Xe^+$ spectrum in the lower trace of Figs. 4(a)–4(e) that the rotational linewidth of the Q-branch transitions increases as the excitation wave number increases. In other words, the predissociation reaction is accelerated by raising the rotational quantum number. This is in agreement with the results expected from the aforementioned rotationally dependent (heterogeneous) interaction between the $C1$ and the $\Omega=0^-$ states.

On the other hand, the spectrum obtained by monitoring the $^{132}Xe^{40}Ar^+$ ions was found to be constructed dominantly from the P- and R-branches. Furthermore, the rotational linewidth, which was substantially larger than the laser bandwidth ($0.09\ \mathrm{cm}^{-1}$), seemed to be independent of the rotational quantum number J'. This finding indicates the presence of another dissociation pathway, originating from the homogeneous coupling ($\Delta\Omega=0$) between the $C1$ state and a nearby electronic state with $\Omega=1$ symmetry. As can be seen in Fig. 1, two $\Omega=1$ states correlating with the low-lying $6s(3/2)_1$ and $6s(3/2)_2$ states of Xe can possibly interact with the $C1$ state to form the low-lying Xe* fragments which cannot be ionized energetically by the ionization laser.

The dissociation process caused by the homogeneous coupling is expected to contribute to the linewidth of the e- and f-parity sublevels by the same amount. Therefore, the rotational linewidth Γ in the $C1$ state can be expressed as

$$\Gamma=\Gamma_0+CJ'(J'+1) \quad \text{for } f\text{-parity sublevels}, \tag{1a}$$

and

$$\Gamma=\Gamma_0 \quad \text{for } e\text{-parity sublevels}, \tag{1b}$$

where Γ_0 describes the width of a rotational line broadening due to the homogeneous dissociation pathway.

C. Quantitative analysis of rotational structures

1. $^{132}Xe^+$ channel

In the preceding subsections, the two dissociation pathways, i.e., the heterogeneous pathways via the $\Omega=0^-$ state and the homogeneous pathway via the $\Omega=1$ states, were proposed on the basis of the two different rotational structures of the respective $C1-X0^+$ transitions, i.e., the rotational structure obtained by monitoring $^{132}XeAr^+$ and that obtained by monitoring $^{132}Xe^+$. In order to derive quantitative information about the dissociation processes, such as the dissociation rates and the branching ratio of these two pathways, a least-squares fit was performed to reproduce the observed partially resolved rotational structures for both of the $XeAr^+$ and Xe^+ spectra.

On the basis of the dissociation mechanism described above, the branching ratio to yield the Xe $6s'(1/2)_0$ fragments is given by $(1-\Gamma_0/\Gamma)$, where the contribution from the radiative decay and the ionization processes is neglected because they are much slower than the dissociation process. Therefore, the rotational structure of the XeAr $C1-X0^+$ $(v',0)$ transition for the $^{132}Xe^+$ channel can be expressed as

$$I_{\mathrm{Xe}}(\nu)=N_{\mathrm{Xe}}\left[\sum_{J''=1} I_Q^{J''}(T)\left(1-\frac{\Gamma_0}{\Gamma}\right)V(\nu,\nu_Q^{J''},\Gamma,\Gamma_{\mathrm{VUV}})\right]+I_{\mathrm{Xe}}^0, \tag{2}$$

where N_{Xe} represents a normalization factor, I_{Xe}^0 a baseline shift relative to an observed spectra, and $I_Q^{J''}$ the Q-branch transition intensity of a rotational level J'' at a rotational temperature T. The factor $(1-\Gamma_0/\Gamma)$ describes the branching ratio to form $^{132}Xe6s'(1/2)_0$ from ^{132}XeAr in the $C1$ state. The function $V(\nu,\nu_Q^{J''},\Gamma,\Gamma_{\mathrm{VUV}})$ represents a normalized Voigt line profile[21] with a peak centered at the Q-branch transition wave number, $\nu_Q^{J''}$. The Voigt profile was defined as a convolution of (i) a Lorentzian line profile with a FWHM width Γ, representing the line broadening by the homogeneous and heterogeneous predissociation processes as given by Eq. (1), and (ii) a Gaussian line profile with a FWHM width, $\Gamma_{\mathrm{VUV}}=0.09\ \mathrm{cm}^{-1}$, representing the spectral bandwidth of the VUV laser.

The simulated rotational structure for the respective $C1-X0^+(v',0)(v'=2-4,6)$ transitions was first fitted to the observed one by a trial-and-error procedure to determine the initial values of the parameters in the least-squares fit. For the (5,0) transition shown in Fig. 4(d), a least-squares analysis was not performed due to the self-absorption effect caused by the strong Xe $[6s'(1/2)_1\leftarrow{}^1S_0]$ resonant transition as described in the following subsection (IIIC2).

In the course of the trial-and-error procedure, it was found necessary to introduce two rotational temperatures, T_1 and $T_2(T_1<T_2)$, to reproduce the intensity patterns of the observed rotational structure. Then the intensity factor for Q-branch transitions was expressed as

$$I_Q^{J''}=S_Q^{J''}\left\{\exp\left[-\frac{F''(J'')}{kT_1}\right]+\alpha\ \exp\left[-\frac{F''(J'')}{kT_2}\right]\right\}, \tag{3}$$

TABLE I. Parameters of the XeAr $C1$ state determined from the least-squares fit to the rotational structures of the C1–X0$^+$ transition obtained by monitoring $^{132}Xe^{40}Ar^+$ and $^{132}Xe^+$ ions.[a]

v'		$B^f_{v'}$	$B^e_{v'}$	$\overline{B_{v'}}$	ν_0	$\overline{\nu_0}$	Γ_0	$\overline{\Gamma_0}$	10^4C	$10^4\overline{C}$
	Xe^+	0.048 27(4)			771 18.60(6)		0.13(1)		2.9(5)	
2				0.048 26(4)		771 18.59(5)		0.14(1)		2.6(5)
	$XeAr^+$	–[b]	0.048 25(5)		771 18.58(3)		0.14(1)		2.1(6)	
	Xe^+	0.047 33(3)			771 37.98(1)		0.15(1)		2.2(4)	
3				0.047 31(4)		771 37.98(1)		0.15(2)		2.2(4)
	$XeAr^+$	–[b]	0.047 28(4)		771 37.98(1)		0.14(3)		2.2(4)	
	Xe^+	0.044 41(2)			771 60.07(1)		0.18(1)		2.5(5)	
4				0.044 43(2)		771 60.08(2)		0.18(2)		2.7(7)
	$XeAr^+$	–[b]	0.044 45(1)		771 60.09(2)		0.19(2)		3.0(8)	
	Xe^+	–			–		–		–	
5				[0.042 41(7)]		[771 84.41(3)]		[0.18(3)]		[3.4(7)]
	$XeAr^+$	–	0.042 41(7)		771 84.41(3)		0.18(3)		3.4(7)	
	Xe^+	0.039 49(4)			772 07.73(2)		0.18(2)		2.4(6)	
6				0.039 51(4)		772 07.71(3)		0.18(2)		2.3(7)
	$XeAr^+$	–[b]	0.039 53(4)		772 07.68(4)		0.17(2)		2.1(7)	

[a]For $v'=5$, the least-squares fit was performed only for the $XeAr^+$ spectra by assuming $B^e_{v'}=B^f_{v'}$.
[b]This value was fixed to $B^f_{v'}$.

where $S_Q^{J''}$ is the Hönl–London factor, and the constant α represents the contribution of the higher temperature T_2. The rotational level energy $F''(J'')$ of the $v''=0$ level in the electronic ground $X0^+$ state was expressed as

$$F''(J'')=B''_0J''(J''+1)-D''_0J''^2(J''+1)^2, \tag{4}$$

where the rotational constants $B''_0=0.032\,0431\ \mathrm{cm}^{-1}$ and the centrifugal distortion constant $D''_0=2.215\,52\times10^{-7}\ \mathrm{cm}^{-1}$ obtained from microwave spectroscopy[22] were adopted. The rotational level energy for the e-parity sublevels $F'_e(J')$ and that for the f-parity sublevels $F'_f(J')$ of the $v'=2-4$ and 6 levels in the $C1$ state were expressed as

$$F'_e(J')=B^e_{v'}J'(J'+1)-D^e_{v'}J'^2(J'+1)^2 \tag{5a}$$

and

$$F'_f(J')=B^f_{v'}J'(J'+1)-D^f_{v'}J'^2(J'+1)^2. \tag{5b}$$

For all the $v'=2-4$ and 6 vibronic levels, the centrifugal distortion constants were fixed to the same value as that of the electronic ground state D''_0, i.e., $D^e_{v'}=D^f_{v'}=2.21552\times10^{-7}\ \mathrm{cm}^{-1}$. In the case of the heterogeneous predissociation from the $C1$ state, only the f-parity sublevels are coupled with a repulsive $\Omega=0^-$ state. Therefore, a total of nine parameters, i.e., ν_0, $B^f_{v'}$, Γ_0, C, T_1, T_2, α, N_{Xe}, I^0_{Xe}, were adopted in the least-squares fit to the rotational structures of the Xe^+ spectra.

Prior to the least-squares fit to the observed rotational contour, the assignments of the rotational quantum number J to the observed Q-branch transition peaks were performed. On the basis of the rotational assignments shown in Figs. 4(a)–4(c) and 4(e), approximate rotational constants $B^f_{v'}$ were derived for the $v'=2-4$ and 6 vibrational levels as initial values for the least-squares fit. The results of the least-squares fits to the observed rotational structures are shown in Figs. 4(a)–4(c) and 4(e). It can be seen in these figures that the best-fit rotational structures reproduce well the experimental results. It was found that the nine parameters were optimized with only small correlations; they are listed in Table I.

2. $^{132}Xe^{40}Ar^+$ channel

The least-squares analyses were also performed for the observed rotational structures for the $^{132}Xe^{40}Ar^+$ spectra in a similar manner as for the $^{132}Xe^+$ spectra. The rotational band of the $^{132}Xe^{40}Ar^+$ spectra consists of all the P-, Q- and R-branch transitions. Since the branching ratios to form $^{132}Xe^{40}Ar^+$ are Γ_0/Γ for the Q branch and 1 for the P- and R-branches, the rotational spectra can be expressed as

$$I_{XeAr}(\nu)=N_{XeAr}\left\{\left[\sum_{J''=1} I_Q^{J''}(T)\left(\frac{\Gamma_0}{\Gamma}\right)V(\nu,\nu_Q^{J''},\Gamma,\Gamma_{VUV})\right]+\left[\sum_{J''=0} I_{P,R}^{J''}(T)V(\nu,\nu_{P,R}^{J''},\Gamma,\Gamma_{VUV})\right]\right\}+I^0_{XeAr}, \tag{6}$$

where the sum in the first square parentheses represents the contribution from the Q-branch transitions, while the sum in the second square parentheses represents the contributions from the P- and R-branch transitions. Using this expression, the least-squares fits of the $^{132}Xe^{40}Ar^+$ spectra were performed. The rotational constant $B^e_{v'}$, the band origin ν_0, the linewidth Γ_0, C, T_1, T_2, and α, N_{XeAr}, and I^0_{XeAr} were used as nine independent variable parameters. The rotational constant, $B^f_{v'}$, was fixed to the value derived from the $^{132}Xe^+$ spectra. The good agreement between the observed and the best-fit rotational structures was achieved for all the $^{132}Xe^{40}Ar^+$ spectra (except $v'=5$) as shown in Figs. 4(a)–4(c) and 4(e). The derived parameters are listed in Table I in comparison with those obtained from the $^{132}Xe^+$ spectra. The determined rotational constants for the e-parity sublevels, $B^e_{v'}$, were found to agree with the rotational constants for the

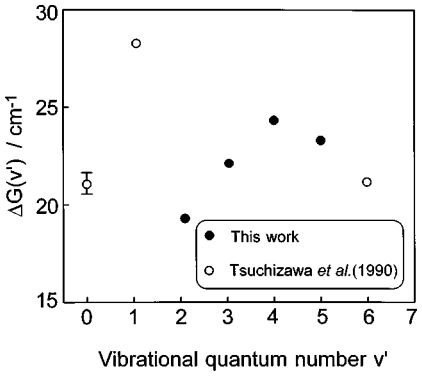

FIG. 5. The dependence of the vibrational energy spacing, $\Delta G(v') = \overline{\nu_0}(v'+1) - \overline{\nu_0}(v')$ $(v'=0-6)$ in the $C1$ state on the vibrational quantum number v'. An irregular behavior can be seen clearly for $\Delta G(v')$ derived both from the present study (filled circle) and from Tsuchizawa *et al.* (Ref. 8) (open circle), which can be attributed to the avoided crossing between the $C1$ state and a nearby repulsive $\Omega=1$ state.

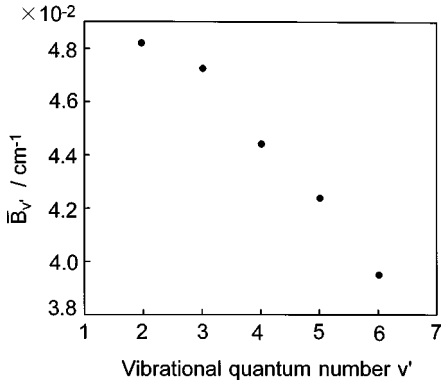

FIG. 6. The weight averaged rotational constants $\overline{B_{v'}}$ in the $C1$ state of XeAr plotted as a function of the vibrational quantum number v'.

f-parity sublevels, $B^f_{v'}$, within their experimental uncertainties, indicating that the Ω-type doubling effect in the $C1$ state is negligibly small.

It should be remarked that a slightly different procedure was adopted for the spectral fit of the (5,0) band. In Fig. 4(d), a large dip can be seen in both of the $^{132}Xe^{40}Ar^+$ and $^{132}Xe^+$ spectra near the rotational band origin region. These large dips were ascribed to the strong absorption of the excitation VUV light by the background Xe atoms due to the intense atomic $[6s'(1/2)_1 \leftarrow {}^1S_0]$ transition located at 771 85.560 cm^{-1}.[15] Since it is difficult to evaluate the extent of the self-absorption and the additional contribution from the $^{132}Xe^+$ ions formed from the ^{132}Xe atoms in the background, the least-squares fit was performed for the $^{132}Xe^{40}Ar^+$ spectrum outside the dip range between the arrows in Fig. 4(d). In the least-squares analysis it was assumed that the e- and f-parity sublevels have the same rotational constants, i.e., $B^f_{v'} = B^e_{v'}$. The optimized seven parameters, $B^e_{v'}$, ν_0, Γ_0, C, T_1, T_2, and α, determined from the least-squares fit for the $^{132}Xe^{40}Ar^+$ (5,0) spectra, were used to simulate the $^{132}Xe^+$ spectra by adjusting the N_{Xe} and I^0_{Xe} factors by a trial-and-error procedure.

3. Vibrational level dependence of the determined parameters

As presented in Table I, the band origin wave numbers ν_0, the line-broadening constants Γ_0 and C determined from the Xe^+ spectra, and the corresponding values determined from the $XeAr^+$ spectra were in good agreement within the experimental uncertainties. This good agreement supports the dissociation mechanism proposed in Sec. IIIB. The weighted averaged values, $\overline{\nu_0}$, $\overline{\Gamma_0}$, $\overline{B_{v'}}$, and $\overline{C}$, were derived from the two corresponding values determined independently from the Xe^+ spectra and the $XeAr^+$ spectra by taking into account their associated uncertainties, and are tabulated also in Table I.

In Fig. 5, the vibrational dependence of the vibrational-level spacing, $\Delta G(v') = \overline{\nu_0}(v'+1) - \overline{\nu_0}(v')$, is plotted. The $\Delta G(v')$ values exhibit irregular behavior as a function of v', indicating that the $C1$ state potential is distorted significantly from a Morse-type potential curve. Previously, Tsuchizawa *et al.*[8] discussed the presence of an avoided crossing between the $C1$ state and a repulsive electronic state with $\Omega=1$ symmetry correlating with the Xe $6s(3/2)_1$ level on the basis of the discontinuity of vibrational term values at around $v'=4$. The irregularity in the vibrational level spacing is seen in Fig. 5 for almost all the vibrational levels, i.e., $v'=2-6$, suggesting that the effect of the distortion of the zero-order diabatic potential by the avoided crossing prevails over a wide energy range.

Figure 6 shows the vibrational dependence of the weighted averaged rotational constants $\overline{B_{v'}}$. It can be seen in this figure that the rotational constants exhibit a zigzag-type deviation from a smooth descendent curve. This irregularity in the rotational constants can also be ascribed to the distortion of the potential curve caused by the avoided crossing, resulting in a change in the vibrational wave function and a certain shift of the rotational constants from their unperturbed values.

The presence of the avoided crossing in the $C1$ state is also reflected in the predissociation process. As shown in Fig. 7(a), the homogeneous predissociation width, Γ_0, increases from $v'=2$ to $v'=4$, and tends to take a constant value for $v' \geqslant 4$. This vibrational dependence can be regarded as the effect of the homogeneous predissociation, induced by the electrostatic coupling with the repulsive part of the $\Omega=1$ state correlating with the $6s(3/2)_1$ or $6s(3/2)_2$ state of Xe.

On the other hand, the off-diagonal matrix element of the rotational Hamiltonian, which couples the $C1$ state with the 0^- state correlating with the Xe $6s'(1/2)_0$ state, could also be affected by the avoided crossing through (i) the change in the electronic character of the $C1$ state near the crossing and/or through (ii) the vibrational overlap factors. In Fig. 7(b) the vibrational dependence of the heterogeneous dissociation parameters, C, are plotted. Though the C value fluctuates to some extent as v' increases, a clear trend is not identified, indicating possibly that the contributions from both of the two factors (i) and (ii) are small in their magnitude, or the effects of these two factors cancel out with each other.

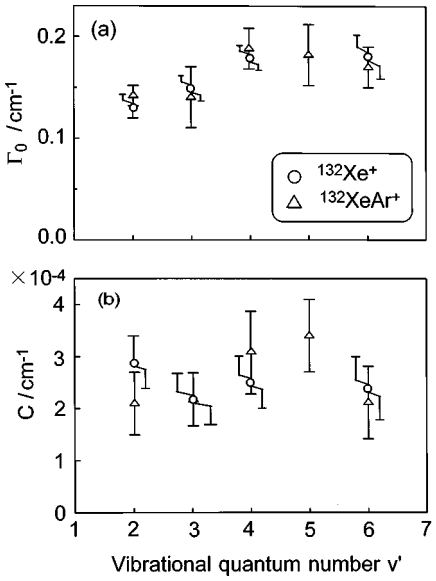

FIG. 7. The homogeneous dissociation rate Γ_0 (a) and the heterogeneous dissociation rate constants C (b) plotted against the vibrational quantum number v'.

IV. SUMMARY

Mass-resolved excitation spectra of the $C1-X0^+$ transition of XeAr in the 130 nm region were measured with high resolution by monitoring both the parent $^{132}Xe^{40}Ar^+$ and fragment $^{132}Xe^+$ ions simultaneously with a reflectron TOF mass spectrometer. The analysis of the rotational structure of the $C1-X0^+(v',0)(v'=2-6)$ bands showed that (i) the detected ^{132}Xe fragments are produced from the heterogenous (rotationally dependent) predissociation through the f-parity sublevels of the $C1$ state of the parent $^{132}Xe^{40}Ar$ molecules, caused by a heterogeneous coupling between the f-parity sublevels of the $C1$ state and the dissociative $\Omega=0^-$ electronic state correlated with the Xe $6s'(1/2)_0$ level, and that (ii) the competing homogeneous (rotationally independent) predissociation pathway exists for both the e- and f-parity sublevels, caused by the avoided curve crossing between the $C1$ state and a nearby repulsive $\Omega=1$ state correlating with either the $6s(3/2)_1$ state or the $6s(3/2)_2$ state of Xe, which are not ionized energetically by the ionization laser ($\lambda=425.11$ nm).

From the least-squares fits to the observed rotational structure for both the $XeAr^+$ spectra and the Xe^+ spectra, the rotational constants, the band origins, the homogeneous dissociation linewidths, and the heterogeneous dissociation constant, were determined for the $(v',0)(v'=2-6)$ vibronic bands as optimized parameters. It was found that the avoided crossing between the potential curves of the $C1$ state and the repulsive $\Omega=1$ state results in the irregular vibrational quantum-number dependence of the vibrational energy spacing, the rotational constants as well as the homogeneous linewidths.

ACKNOWLEDGMENTS

The present work is supported partly by the Research Fund (for Selected Area) from the College of Arts and Sciences, the University of Tokyo, Grant-in-Aid for Scientific Research (#05453016, #08640636) and Grant-in-Aid for Scientific Research on Priority Area (#07240106) from the Ministry of Education, Science, Sports, and Culture, and CREST (Core Research for Evolutionary Science and Technology) fund from Japan Science Technology Corporation. S.L. acknowledges financial support from the Japanese Government (Monbusho) Scholarship.

[1] P. R. Herman, P. E. LaRocque, and B. P. Stoicheff, J. Chem. Phys. **89**, 4535 (1988), and references therein.
[2] K. Tsukiyama and T. Kasuya, J. Mol. Spectrosc. **151**, 312 (1992).
[3] C. D. Pibel, K. Yamanouchi, and S. Tsuchiya, J. Chem. Phys. **100**, 6153 (1994).
[4] S. S. Dimov, J. Y. Cai, and R. H. Lipson, J. Chem. Phys. **101**, 10313 (1994); S. S. Dimov, X. K. Hu, D. M. Mao, and R. H. Lipson, Chem. Phys. Lett. **239**, 332 (1995); X. K. Hu, D. M. Mao, S. S. Dimov, and R. H. Lipson, Chem. Phys. **201**, 557 (1995); R. H. Lipson, S. S. Dimov, J. Y. Cai, P. Wang, and H. A. Bascal, J. Chem. Phys. **102**, 5881 (1995); D. M. Mao, X. K. Hu, S. S. Dimov, and R. H. Lipson, J. Mol. Spectrosc. **181**, 435 (1997); X. K. Hu, D. M. Mao, S. S. Dimov, and R. H. Lipson, J. Chem. Phys. **106**, 9411 (1997).
[5] M. C. Castex, J. Chem. Phys. **66**, 3854 (1977).
[6] D. E. Freeman, K. Yoshino, and Y. Tanaka, J. Chem. Phys. **67**, 3462 (1977).
[7] S. T. Pratt, P. M. Dehmer, and J. L. Dehmer, J. Chem. Phys. **83**, 5380 (1985).
[8] T. Tsuchizawa, K. Yamanouchi, and S. Tsuchiya, J. Chem. Phys. **92**, 1560 (1990).
[9] C. D. Pibel, K. Yamanouchi, J. Miyawaki, S. Tsuchiya, B. Rajaram, and R. W. Field, J. Chem. Phys. **101**, 10242 (1994).
[10] R. H. Lipson, S. S. Dimov, X. K. Xu, D. M. Mao, and Y. J. Cai, J. Chem. Phys. **103**, 6313 (1995).
[11] S. S. Dimov, X. K. Hu, D. M. Mao, J. Y. Cai, and R. H. Lipson, J. Chem. Phys. **104**, 1213 (1996).
[12] C. D. Pibel, K. Ohde, and K. Yamanouchi, J. Chem. Phys. **105**, 1825 (1996).
[13] D. M. Mao, X. K. Hu, S. S. Dimov, and R. H. Lipson, J. Phys. B **29**, L89 (1996).
[14] K. Yamanouchi, and S. Tsuchiya, J. Phys. B **23**, 133 (1995).
[15] C. E. Moore, *Atomic Energy Levels*, NBS Circ. 467, Vol. II (Washington, D. C., 1952).
[16] S. G. Tilford and J. D. Simmons, J. Phys. Chem. Ref. Data **1**, 147 (1972).
[17] S. Gestenkorn and P. Luc, *Altas du Spectre d'Absorption de la Molecule d'Iode* (Edition du centre National la Researche Scientifique, Paris, 1978).
[18] K. Tsukiyama, M. Tsukakosi, and T. Kasuya, Chem. Phys. **127**, 393 (1988).
[19] H. Lefebvre-Brion and R. W. Field, *Perturbations in the Spectra of Diatomic Molecules* (Academic, London, 1986).
[20] A. P. Hickman, D. L. Huestis, and R. P. Saxon, J. Chem. Phys. **96**, 2099 (1992).
[21] F. Schreier, J. Quant. Spectrosc. Radiat. Transf. **48**, 743 (1992).
[22] W. Jager, Y. Xu, and M. C. Gerry, J. Chem. Phys. **99**, 919 (1993).